ACS APPLIED MATERIALS & INTERFACES

Research Article

www.acsami.org

Mesoporous $Ni_{0.85}Se$ Nanospheres Grown in Situ on Graphene with High Performance in Dye-Sensitized Solar Cells

Xiao Zhang,[†] Yuxiao Yang,[†] Shengqi Guo,[†] Fangzhong Hu,*[,‡] and Lu Liu*[,†]

[†]Tianjin Key Laboratory of Environmental Remediation and Pollution Control, College of Environmental Science and Engineering and [‡]State Key Laboratory and Institute of Elemento-Organic Chemistry, Nankai University, Tianjin 300071, P. R. China

Supporting Information

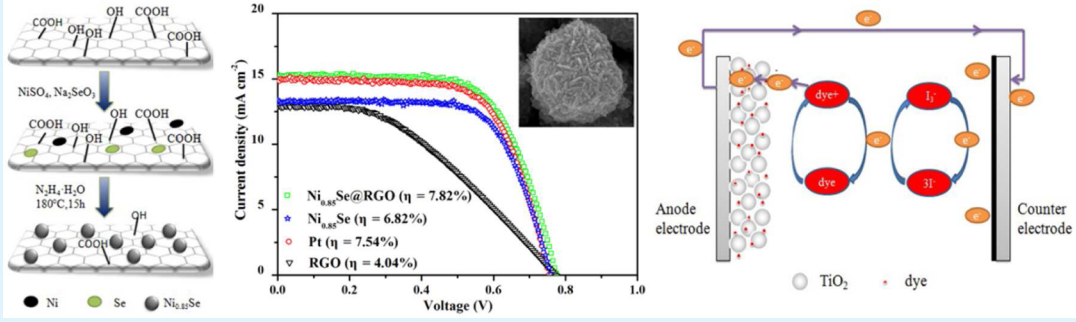

ABSTRACT: Mesoporous $Ni_{0.85}Se$ nanospheres grown on graphene were synthesized via the hydrothermal approach. Because of the exceptional electron-transfer pathway of graphene and the excellent catalytic ability of the mesoporous $Ni_{0.85}Se$ nanospheres, the nanocomposites exhibited excellent electrocatalytic property as the counter electrode (CE) of dye-sensitized solar cells. More catalytic active sites, better charge-transfer ability and faster reaction velocity of $Ni_{0.85}Se$@RGO (RGO = reduced graphene oxide) CE led to faster and more complete I_3^- reduction than Pt, $Ni_{0.85}Se$, and RGO CEs. Furthermore, the power conversion efficiency of $Ni_{0.85}Se$@RGO CE reached 7.82%, which is higher than that of Pt CE (7.54%). Electrochemical impedance spectra, cyclic voltammetry, and Tafel polarization were obtained to demonstrate positive synergetic effect between $Ni_{0.85}Se$ and RGO, as well as the higher catalytic activity and the better charge-transfer ability of $Ni_{0.85}Se$@RGO compared with Pt CE.

KEYWORDS: *$Ni_{0.85}Se$, mesoporous nanospheres, graphene, DSSCs*

1. INTRODUCTION

In recent years, optimal counter electrode (CE) materials with low cost, high catalytic activity, and great resource abundance for dye-sensitized solar cells (DSSCs) have attracted much research attention.[1−6] As a component playing a significant role in DSSC, CE collects electrons from external circuit and fulfills electron transfer from the CE interface to the electrolyte, then provides activation energy for the regeneration of I^- from I_3^-.[7−9] These processes are decisive to the effective utilization of photogenerated electrons and circular reaction of electrolyte; furthermore, they specifically influence the short-circuit current (J_{sc}), fill factor (FF), and power conversion efficiency (PCE). To obtain excellent photovoltaic property, the materials used in CE should possess the following advantages: low charge resistance, high catalytic activity, and good chemical stability in the electrolytic cell system.[10−12] High chemical stability can effectively prevent CEs from being corroded by electrolyte. Because of the encouraging electrocatalytic activity for reducing I_3^-, platinum (Pt) is recognized to be an efficient CE catalytic material. However, as a scarce metal, Pt is expensive for mass production. Besides, electrolyte can easily corrode Pt to PtI_4 and H_2PtI_6, worsening the CE performance.[13] Given the above restrictions, many low-cost and efficient materials have been proposed to replace Pt, such as carbonaceous materials,[14−17] metal oxides,[18−20] sulfides,[21−24] nitrides,[25,26] chalcogenides,[7,27,28] and polymers.[29]

As the thinnest two-dimensional (2D) material, graphene possesses high carrier mobility (>200 000 $cm^2\ V^{-1}\ s^{-1}$ at an electron density of 4×10^{-9} cm^{-2}), large specific surface area (2600 $m^2\ g^{-1}$), and excellent thermal/chemical stability.[30−34] Furthermore, interconnected graphene can capture the injected electrons and work as the "speedway" to enhance the electron-transport rate of nanomaterials.[35,36] On the basis of the above characteristics, graphene has been considered to be an ideal substrate for the growth of functional nanomaterials applied in CEs of DSSCs. Recent research showed that metal and inorganic nanomaterials, such as Pt, Ni, carbon nanotube, and TiO_2, grown on graphene, can be viable replacements for Pt.[37−40] Misra et al. combined graphene with nickel nanoparticle, and the catalytic efficiency surpassed that of Pt.[39] Chen et al. synthesized three-dimensional single-walled carbon

Received: November 26, 2014
Accepted: April 8, 2015
Published: April 8, 2015

DOI: 10.1021/acsami.5b00464
ACS Appl. Mater. Interfaces 2015, 7, 8457−8464

nanotube/graphene composites and demonstrated that the composites have great potential for DSSC-related applications.[38]

As an important class of chalcogenides, $Ni_{0.85}Se$ possesses distinctive electronic configuration and comparatively high catalytic activity. Recent studies have demonstrated that $Ni_{0.85}Se$ presented good electrocatalytic performance for the triiodide reduction and can be a potential material as CEs.[11,41] On the other hand, excellent morphology of CE materials can also improve the electrocatalytic performance. It is well-known that the mesoporous structure can provide large surface area, fast electron transfer channels, and many catalytic active sites.[42−44] Furthermore, the mesoporous structure assembled from nanoplates can accommodate I_3^- molecules among nanoplates, thus increasing the collision between I_3^- and catalytic active sites. However, electrocatalytic property of mesoporous $Ni_{0.85}Se$ grown in situ on graphene as CEs has not been investigated.

Herein, we report a facile approach to synthesize mesoporous $Ni_{0.85}Se$ nanospheres on reduced graphene oxide ($Ni_{0.85}Se$@RGO) and test its performance as the CE of DSSCs. In possession of both exceptional electron-transfer pathway of graphene and excellent catalytic ability of the mesoporous $Ni_{0.85}Se$ nanospheres, $Ni_{0.85}Se$@RGO CE exhibited a fairly high PCE of 7.82%, outperforming pure $Ni_{0.85}Se$ (6.82%), and RGO (4.04%), even better than Pt CE (7.54%). To the best of our knowledge, it is the first exploration of the application of mesoporous $Ni_{0.85}Se$ nanospheres@graphene nanocomposites in DSSCs.

2. EXPERIMENTAL SECTION

Synthesis of GO Nanosheets. Graphene oxide (GO) nanosheets were prepared by a modified Hummers method.[45] In detail, graphite powder (2 g) was put into 100 mL cooled (0 °C) concentrated H_2SO_4. Following the slow addition of $KMnO_4$ (6 g), a slight exotherm may be produced in this process. The suspension was then stirred at 35 °C for 12−15 h. Afterward, 200 mL of distilled water was added, and the temperature was kept at 96 °C for 2 h. The temperature was reduced to 60 °C, and H_2O_2 (30%, 10 mL) was injected into the suspension to completely react with the excess $KMnO_4$, which yielded a bright yellow mixture. The solid product was separated by centrifugation and then washed with HCl (5%) several times with water until the pH value of the supernatant was nearly 6, and GO was obtained. The collected precipitate was dispersed in water, then sonicated, subsequently concentrated to obtain a GO suspension, and kept at 50 °C for 10 h, and GO powder was obtained.

Synthesis of $Ni_{0.85}Se$@RGO. All reagents are of analytic grade and used without further purification. The whole experimental flowchart is schematically illustrated in Figure 1. The synthesis method is a modified strategy of Li et al.[46] In detail, $Ni_{0.85}Se$@RGO was prepared via a hydrothermal reaction using $NiSO_4{\cdot}7H_2O$ and $Na_2SeO_3{\cdot}5H_2O$ as Ni and Se sources, respectively, in the presence of ethylenediaminetetraacetic acid (EDTA) as chelating agent and deionized water as solvent. First, 0.2628 g of $NiSO_4{\cdot}7H_2O$, 1.0 g of EDTA, and 5 mL of GO water suspension (10 mg/mL) were dissolved in 25 mL of deionized water in a 50 mL Teflon-lined autoclave. Then 1.0 g of NaOH was added to keep the pH value at ∼14. After this mixture was stirred for 1 h, 0.789 g of $Na_2SeO_3{\cdot}5H_2O$ was added to the mixture. Lastly, 3 mL of hydrazine hydrate was added to reduce Na_2SeO_3 and GO. After this mixture was stirred for 5 min, the autoclave was sealed and heated at 180 °C for 15 h. Then, the autoclave was allowed to cool to room temperature naturally. The $Ni_{0.85}Se$@RGO product was washed with water and absolute ethanol to remove impurities and then dried at 60 °C. The pure $Ni_{0.85}Se$ nanospheres were obtained under the same reaction conditions in the absence of GO.

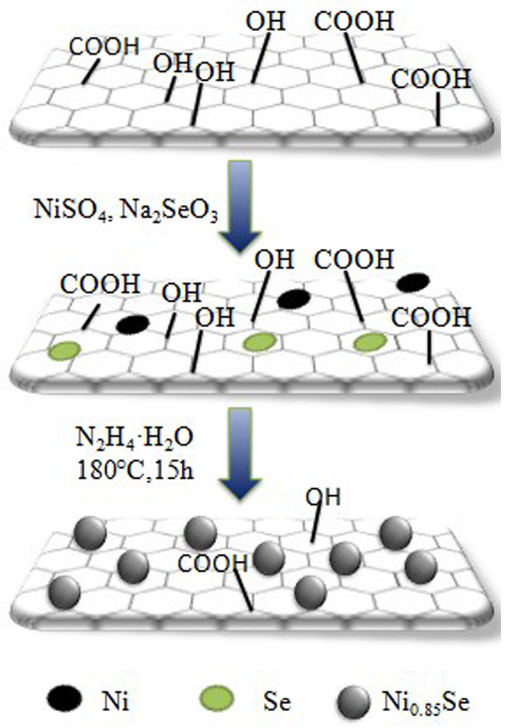

Figure 1. Formation process of the mesoporous $Ni_{0.85}Se$@RGO nanospheres.

Characterization of Obtained Samples. The crystallinity and composition of the samples were characterized by X-ray diffraction (XRD, D/max-2500, Japan Science) with Cu Kα radiation (λ = 1.540 56 Å). The morphology of samples was studied by field-emission scanning electron microscopy (FE-SEM, Nanosem 430, FEI). More detailed insight into the microstructure of the sample was given by high-resolution transmission electron microscopy (HRTEM, Tecnai G2 F20, operating at 200 kV, FEI) equipped with energy-dispersion spectroscopy (EDS) to measure the elements in the samples. The Brunauer−Emmett−Teller (BET) specific surface area was analyzed by the BET equation using a Tristar 3000 nitrogen adsorption apparatus.

Fabrication of Dye-Sensitized Solar Cells. $Ni_{0.85}Se$@RGO slurry was made in ethanol by mixing 0.1 g of $Ni_{0.85}Se$@RGO powder with 0.025 g of PEG20000 and stirred continuously. Then a film was made by wiping $Ni_{0.85}Se$@RGO slurry on fluorine-doped tin oxide (FTO) conductive glass (LOF, TEC-15, 15 W per square) with a doctor-blade. After the film was steady, the conductive glass with film was heated at 450 °C for 2 h under the protection of argon to get the $Ni_{0.85}Se$@RGO CE.

A commercial TiO_2 sol (Solaronix, Ti-Nanoxide T/SP) was used to prepare the TiO_2 film on FTO also by the aforementioned method, and the film was soaked in an N719 dye solution (in ethanol) for 24 h to obtain dye-sensitized TiO_2 electrodes. DSSCs were assembled by injecting the electrolyte into the aperture between the dye-sensitized TiO_2 electrode and the CE. The liquid electrolyte is composed of 0.05 M I_2, 0.1 M LiI, 0.6 M 1, 2-dimethyl-3-propylimidazolium iodide (DMPII), and 0.5 M 4-*tert*-butylpyridine with acetonitrile as the solvent. Surlyn 1702 was used as the spacer between the two electrodes. The two electrodes were clipped together with solid paraffin working as the sealant to prevent the electrolyte solution from leaking. The effective cell area was 0.25 cm^2. For comparison, other DSSCs were fabricated by replacing $Ni_{0.85}Se$@RGO with $Ni_{0.85}Se$, RGO, and Pt with other procedures remaining the same. The standard Pt CE was purchased from Dalian Heptachroma Solar Tech Co., Ltd.

Characterization of the Counter Electrodes and Dye-Sensitized Solar Cells. All the electrochemical properties were measured with the Zahner IM6 exelectrochemical workstation.

DOI: 10.1021/acsami.5b00464
ACS Appl. Mater. Interfaces 2015, 7, 8457−8464

Photocurrent−voltage curves were conducted in simulated AM 1.5 illumination (100 mW cm^{-2}, Trusttech CHF-XM-500W) with a Keithley digital source meter (Keithley 2410, USA). Cyclic voltammetry (CV) was recorded with a three electrode system on the exelectrochemical workstation. Pt was used as the CE, and Ag/AgCl was used as the reference electrode. A solution of 10.0 mM LiI, 1.0 mM I_2, and 0.1 M $LiClO_4$ in acetonitrile served as the electrolyte. CV curves were recorded in the range from −0.4 to 1.2 V at a scan rate of 25 mV s^{-1}. Electrochemical impedance spectra (EIS) analysis was conducted at zero bias potential, and the impedance data covered a frequency range of 0.1 Hz−1 MHz. The amplitude of the sinusoidal alternating current voltage signal was 5 mV. The analyses of the resulting impedance spectra were conducted using the software Zview 2.0. Tafel-polarization measurements were employed in a symmetrical dummy cell, which was used in the EIS experiments. The electrolyte was the same as the electrolyte of DSSC. The scan rate was 20 mV s^{-1}, and the voltage range is from −1.0 to 1.0 V.

3. RESULTS AND DISCUSSION

X-ray Diffraction Analysis of GO, RGO, $Ni_{0.85}Se$, and $Ni_{0.85}Se$@RGO. Figure 2 shows the XRD patterns of GO, RGO, $Ni_{0.85}Se$, and $Ni_{0.85}Se$@RGO. In general, GO showed a significant (002) peak at 10.02°, a *d*-spacing of 0.882 nm. As GO was reduced to RGO by hydrazine hydrate, the (002) graphite peak shifted to a larger angle of 23.6° with a *d*-spacing of 0.378 nm. The large interlayer distance of the GO was attributed to the presence of hydroxyl, epoxy, and carboxyl groups.[47,48] All the diffraction peaks of the as-prepared $Ni_{0.85}Se$ and $Ni_{0.85}Se$@RGO samples could be well-indexed to $Ni_{0.85}Se$ (JCPDS No. 18−0888, vertical line in Figure 2), and there is no obvious peak shift compared with $Ni_{0.85}Se$ standard card, which indicates that the atomic ratio of Ni and Se does not deviate from 0.85:1 and other nickel selenides (NiSe or Ni_3Se_4, etc.) do not exist. No characteristic peak was observed for other impurities such as Ni, Se, and NiO. All peaks can be assigned to the (101), (102), (110), (103), (201), and (202) planes of the $Ni_{0.85}Se$, respectively. These manifest that pure crystalline $Ni_{0.85}Se$ and $Ni_{0.85}Se$@RGO were successfully formed via the hydrothermal process.

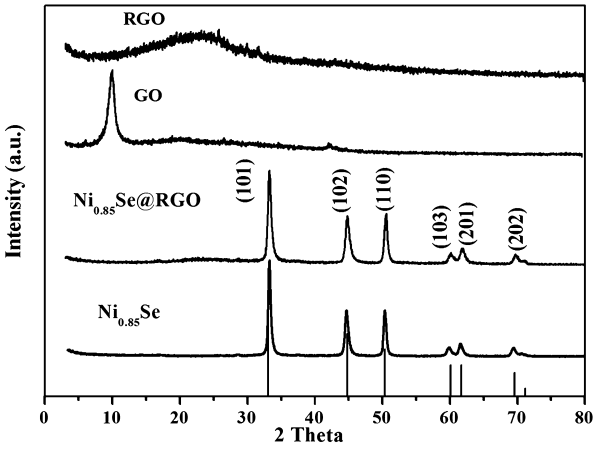

Figure 2. XRD patterns of GO, RGO, $Ni_{0.85}Se$, and $Ni_{0.85}Se$@RGO samples.

Scanning Electron Microscopy Analysis of $Ni_{0.85}Se$@RGO. The structural details of the $Ni_{0.85}Se$@RGO hybrids were investigated by SEM and TEM. The $Ni_{0.85}Se$@RGO was typical of nanospheres with an average diameter of ∼500 nm, as shown in Figure 3a and Supporting Information, Figure S1a. Higher-magnification SEM image (Figure 3b) reveals that the surface

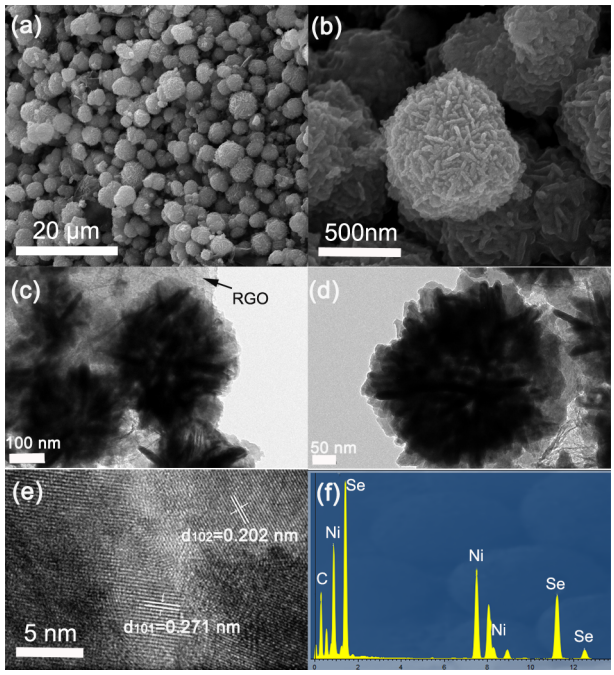

Figure 3. Typical SEM (a, b), TEM (c, d), HRTEM (e), and EDS (f) images of mesoporous $Ni_{0.85}Se$@RGO nanospheres.

of the $Ni_{0.85}Se$ nanospheres is not smooth. And $Ni_{0.85}Se$ nanospheres are built of many nanoplates, which make the spheres look very rugged and contain many pores. These nanoplates contain many active catalytic sites, endowing the nanospheres with large surface area and good electrocatalytic activity.[46] SEM image of $Ni_{0.85}Se$ nanospheres is shown in Supporting Information, Figure S2. More detailed insight into the microstructure of the sample was given by TEM and HRTEM investigation.

Transmission Electron Microscopy Analysis of $Ni_{0.85}Se$@RGO. The TEM images in Figure 3c,d further reveal that $Ni_{0.85}Se$ is well-defined nanoplates-constituted nanospheres structure. Meanwhile, the obvious contrast between the bright mesopores and the relatively dark nanoplates confirmed the mesoporous nature. From Figure 3a and Supporting Information, Figure S1b, the other apparent contrast can be observed between the gray edge portion and dark spheres, which reveals that the spheres were formed on graphene sheets. The lattice spacing (Figure 3e) of 0.202 nm corresponds to the *d*-spacing between adjacent (102) crystallographic planes of the $Ni_{0.85}Se$ nanospheres, and accordingly the fringes of d = 0.271 nm match the (101) plane. EDS profile indicates the existence of three elements: C, Ni, Se (Figure 3f). The C peak is from the graphene, while the Ni and Se peaks are from $Ni_{0.85}Se$. The TEM images of graphene are shown in Supporting Information, Figure S3.

Brunauer−Emmett−Teller Analysis of $Ni_{0.85}Se$/RGO. The BET specific surface area of the $Ni_{0.85}Se$@RGO sample was investigated by nitrogen adsorption and desorption isotherms. Figure 4 displays the nitrogen absorption−desorption isotherms and the pore size distribution (inset in Figure 4). The isotherm can be categorized as type IV with a distinct hysteresis loop observed in the range of 0.5−1.0 P/P_0, which is the characteristic of mesoporous materials. The BET specific surface area of the sample was calculated from N_2 isotherms at 77 K and was found to be as much as ∼63.37 m^2

DOI: 10.1021/acsami.5b00464
ACS Appl. Mater. Interfaces 2015, 7, 8457−8464

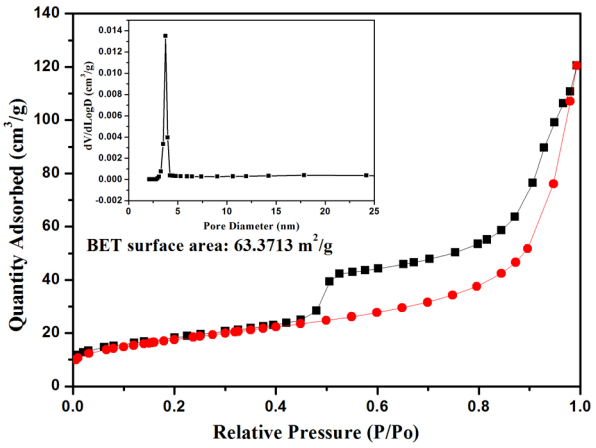

Figure 4. N_2 adsorption/desorption isotherm and Barrett–Joyner–Halenda pore size distribution plot (inset) of $Ni_{0.85}Se$@RGO.

g^{-1}, which is large enough to enable the mesoporous nanospheres host to provide many active sites and adsorption sites. The pore size distribution data indicate that a majority of the pores are ~3–5 nm, determined by the Barrett–Joyner–Halenda (BJH) method. The BET surface area and the pore size strongly indicate that the as-prepared nanospheres have a mesoporous structure.

Dye-Sensitized Solar Cell Performance Analysis of Different Counter Electrodes. To elucidate the catalytic activities and charge-transfer abilities of different CEs on the reduction of triiodide, electrochemical impedance spectra (EIS) experiments were performed using symmetric cells fabricated with two identical electrodes (CE/electrolyte/CE). The EIS of various symmetric CEs can provide the data about the impedance properties, namely, series resistance (R_s), charge-transfer resistance (R_{ct}), and Nernst diffusion impedance (Z_N).[49] The obtained parameters can be calculated from the fitting results of the equivalent circuit, as shown in the inset of Figure 5, and the relevant values are summarized in Table 1. In the higher frequency regions of the Nyquist plots (Figure 5), R_s and R_{ct} can be obtained. The R_s values of $Ni_{0.85}Se$@RGO, $Ni_{0.85}Se$, Pt, and RGO were 23.03, 23.62, 22.60, and 22.03 Ω, respectively. The smaller R_s values are probably caused by the

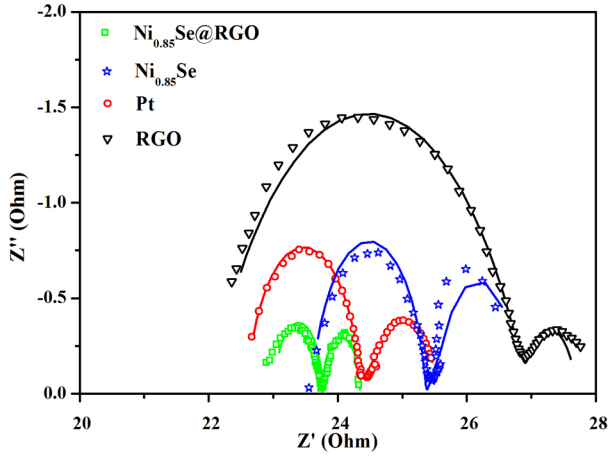

Figure 5. Nyquist plots for symmetric cells fabricated with $Ni_{0.85}Se$@RGO, $Ni_{0.85}Se$, Pt, and RGO CEs. The lines express fit results for corresponding EIS data, and the inset gives the equivalent circuit.

Table 1. Corresponding Values of Series Resistance (R_s), Charge-Transfer Resistance (R_{ct}), Nernst Diffusion Impedance (Z_N), and Peak-to-Peak Separation (E_{pp})

CEs	R_s (ohm)	R_{ct} (ohm)	Z_N (ohm)	E_{pp} (mV)
$Ni_{0.85}Se$@RGO	23.03	0.39	0.59	242
$Ni_{0.85}Se$	23.62	1.76	1.88	239
Pt	22.60	0.90	0.66	429
RGO	22.03	2.45	0.99	

fact that the purchased Pt commercial electrode is very thin. For graphene, which possesses the thinnest 2D nanostructure, the R_s value is smallest. Benefiting from large surface area and fast electron transfer channels, the R_{ct} and Z_N values of $Ni_{0.85}Se$@RGO CE were smaller than those of $Ni_{0.85}Se$ and Pt CE. Smaller R_{ct} value of $Ni_{0.85}Se$@RGO (0.39 Ω), compared with that of $Ni_{0.85}Se$ (1.76 Ω), Pt (0.90 Ω), and RGO (2.45 Ω), implied better electrocatalytic activity on the reduction of triiodide.[43] Similarly, the Z_N value of $Ni_{0.85}Se$@RGO (0.59 Ω) was the smallest among the CEs, which represented the bigger diffusion coefficients and faster transfer speed of triiodide than the other CEs.[50] In summary, the R_{ct} and Z_N values of $Ni_{0.85}Se$@RGO CE reflect the enhancement of charge-transfer ability and electrolyte molecular diffusion rate resulting from the graphene. And the EIS measurement demonstrated that $Ni_{0.85}Se$@RGO CE had better catalytic activities and charge-transfer abilities than Pt.

To investigate reaction kinetics and electrocatalytic activities of the as-prepared $Ni_{0.85}Se$@RGO, $Ni_{0.85}Se$, Pt, and RGO CEs toward the reduction of I_3^-, cyclic voltammetry (CV) was measured with a three-electrode system. As shown in Figure 6,

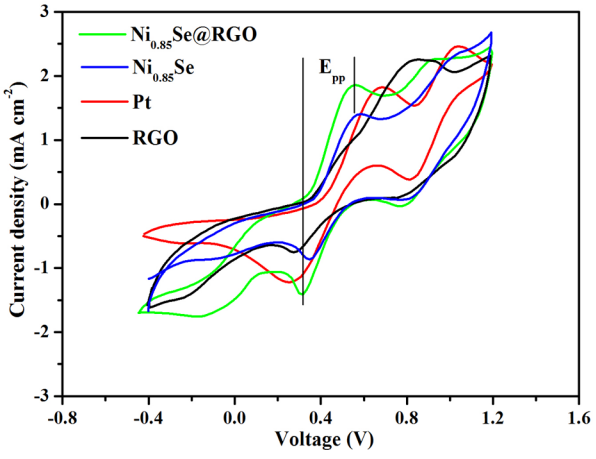

Figure 6. CV curves of iodide/triiodide redox species for $Ni_{0.85}Se$@RGO, $Ni_{0.85}Se$, RGO, and Pt CEs at a scan rate of 25 mV s^{-1}, and the voltage range is from −0.4 to 1.2 V.

all the curves exhibit two typical pairs of oxidation–reduction peaks. The relative negative pair is assigned to the oxidation and reduction of I^-/I_3^- (eq 1), whereas the positive pair is assigned to the oxidation and reduction of I_2/I_3^- (eq 2).

$$I_3^- + 2e \leftrightarrow 3I^- \quad (1)$$

$$3I_2 + 2e \leftrightarrow 2I_3^- \quad (2)$$

Peak current intensity and peak-to-peak separation (E_{pp}) are two important parameters for comparing catalytic activities of different CEs. The higher cathodic peak current density reveals

DOI: 10.1021/acsami.5b00464
ACS Appl. Mater. Interfaces 2015, 7, 8457–8464

the faster reduction velocity, and the smaller peak-to-peak separation (E_{pp}) reflects the better reversibility of the redox reaction.[51] The E_{pp} value is negatively correlated with the standard electrochemical rate constant of a redox reaction,[27] and the E_{pp} values of $Ni_{0.85}Se$@RGO (242 mV) and $Ni_{0.85}Se$ (239 mV) were much smaller than that of Pt CE (429 mV). Furthermore, the cathodic peak current density of $Ni_{0.85}Se$@RGO CE was higher than those of $Ni_{0.85}Se$ and Pt CEs, whereas the cathodic peak of the RGO CE was almost absent in the scan range. The higher cathodic peak current densities and lower E_{pp} value (Table 1) also revealed that catalytic activity for the reduction of I_3^- of $Ni_{0.85}Se$@RGO CE is remarkable, even better than the Pt electrode. Compared with $Ni_{0.85}Se$, $Ni_{0.85}Se$@RGO CE owned similar value of E_{pp}. However, the cathodic peak current density of $Ni_{0.85}Se$@RGO CE was higher than that of $Ni_{0.85}Se$, which was perhaps caused by the synergistic effect between $Ni_{0.85}Se$ and RGO. The CV data show that the addition of graphene did not increase overpotential loss but improved the reaction velocity of CE materials.

Figure 7 gives the Tafel polarization curves performed on the symmetric cells used in the EIS experiments, and it is a

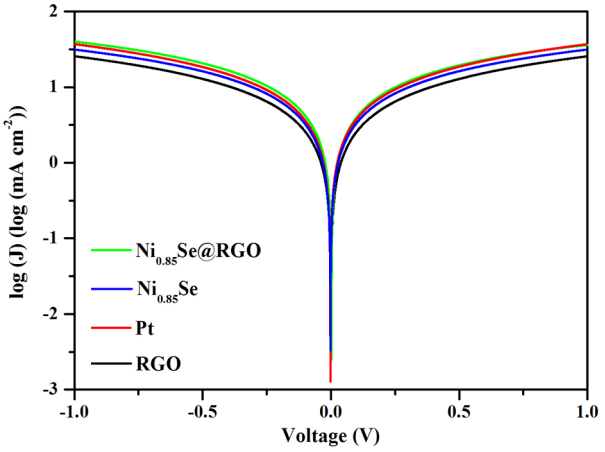

Figure 7. Tafel polarization curves of I^-/I_3^- symmetrical cells of $Ni_{0.85}Se$@RGO, $Ni_{0.85}Se$, Pt, and RGO.

powerful electrochemical characterization method to examine catalytic activity for reducing I_3^- and diffusion coefficient of I_3^-. The Tafel curve includes anodic and cathodic branches; in addition, it can be divided into three zones: polarization zone (low potential, $|V| < 120$ mv), Tafel zone (intermediate potential with a sharp slope), and diffusion zone (high potential). The Tafel curve provides information about the exchange current density (J_0), which has a close positive correlation with the catalytic activity for reducing I_3^-. J_0 is in inverse proportion to R_{ct} based on eq 3, and it could be also obtained by intersecting the cathodic branch and the equilibrium potential line (Supporting Information, Figure S4). The J_0 values of as-prepared CEs were in the order of $Ni_{0.85}Se$@RGO > Pt > $Ni_{0.85}Se$ > RGO, and this sequence also proved that $Ni_{0.85}Se$@RGO owned the best catalytic activities among the three CEs.

$$J_0 = \frac{RT}{nfR_{ct}} \quad (3)$$

where R is the gas constant, T is the temperature, f is Faraday's constant, n is the total number of electrons involved in the reaction, and R_{ct} is the charge transfer resistance.

Table 2. Corresponding Values of Open-Circuit Voltage (V_{oc}), Short-Circuit Current (J_{sc}), Fill Factor (FF), and Power Conversion Efficiency (η)

CEs	V_{oc} (V)	J_{sc} (mA cm^{-2})	FF	η (%)
$Ni_{0.85}Se$@RGO	0.78 ± 0.04	15.20 ± 1.2	0.66 ± 0.02	7.82 ± 0.07
$Ni_{0.85}Se$	0.76 ± 0.02	13.20 ± 0.8	0.68 ± 0.04	6.82 ± 0.19
Pt	0.76 ± 0.02	14.80 ± 0.4	0.67 ± 0.02	7.54 ± 0.13
RGO	0.77 ± 0.04	12.81 ± 2.4	0.41 ± 0.03	4.04 ± 0.7

The schematic diagram about the work principle of DSSC is shown in Figure 8a. In the diagram, CBM is conduction-band minimum, D* is excited dye molecule, D is dye molecule, E_{CB} is conduction band energy, E_f is Fermi energy, and E_{VB} is valence band energy. In the power conversion process, the excited dye molecules release photogenerated electrons to the conduction band of photoanode materials. After the electrons flow through external circuit to CE, CE materials at the interface give electrons to I_3^-.[52] The transfer of electrons in CE is very interesting, and how the CE materials give the electrons to I_3^- is worthy of study.

Figure 8b compares the photovoltaic performance of N719-sensitized solar cells assembled with four CEs ($Ni_{0.85}Se$@RGO, $Ni_{0.85}Se$, Pt, and RGO), and Table 1 shows the corresponding photovoltaic parameters. Open-circuit voltage (V_{oc}) values of $Ni_{0.85}Se$@RGO and Pt CE are similar because it is mostly controlled by the photoanode and electrolyte. Compared with the PCE of Pt CE (η = 7.54%), the DSSC with $Ni_{0.85}Se$@RGO CE exhibited higher PCE (η = 7.82%). This improvement can be visually attributed to the higher current intensity, and in Figure 8 the curve of $Ni_{0.85}Se$@RGO is higher and more stable than other CEs before 0.5 V. The current intensity can be affected by illumination intensity, photoanode, and R_s. In our experiment, illumination intensity and photoanode were same for CEs. Furthermore, the R_s value of $Ni_{0.85}Se$@RGO CE was bigger than that of Pt (R_s correlates inversely with current intensity). From the perspective of reaction mechanism in CEs, more catalytic active sites, higher catalytic activity, and better charge-transfer ability of $Ni_{0.85}Se$@RGO CE lead to the fact that the reduction of I_3^- will be faster and more complete, and photogenerated electron transfer at the CE/electrolyte interface will be enhanced. Therefore, the DSSC assembled with $Ni_{0.85}Se$@RGO CE exhibited higher current intensity. On the other hand, the J_{sc} (13.20 mA cm^{-2}) and PCE (6.82%) values of $Ni_{0.85}Se$ CE are both lower than those of $Ni_{0.85}Se$@RGO CE. As to RGO, there is limited number of active sites in its basal plane for I_3^- electrocatalysis, and the 2D structure of graphene leads to weak adhesion to conductive substrate,[53] resulting in low J_{sc} (12.81 mA cm^{-2}), FF (0.41), and PCE (4.04%) values. These results demonstrated the synergetic catalysis between $Ni_{0.85}Se$ and graphene, as well as the improved photovoltaic performance of CE materials resulting from graphene.

To evaluate electrochemical stability of the $Ni_{0.85}Se$@RGO CE, as shown in Figure 9, consecutive CV experiments were performed at a scan rate of 25 mV s^{-1}. After 20 cycles of scanning, there was negligible change in peak current density and E_{pp}. This further demonstrated that the $Ni_{0.85}Se$@RGO CE owned not only low charge resistance, good catalytic activity,

DOI: 10.1021/acsami.5b00464
ACS Appl. Mater. Interfaces 2015, 7, 8457−8464

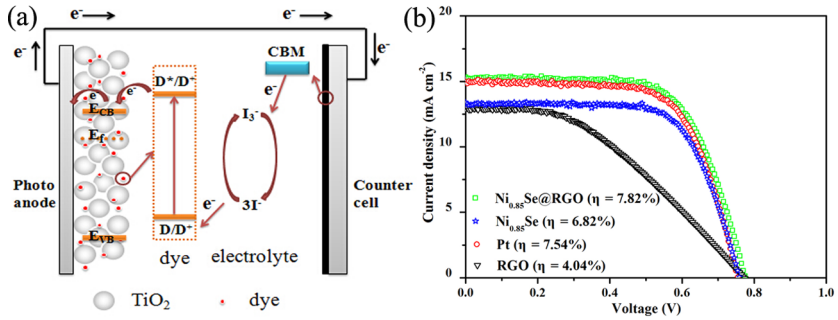

Figure 8. Schematic diagram about the work principle of DSSC (a). Photocurrent density−voltage characteristics of DSSCs with different CEs, measured at AM1.5G illumination (100 mW cm^{-2}) (b).

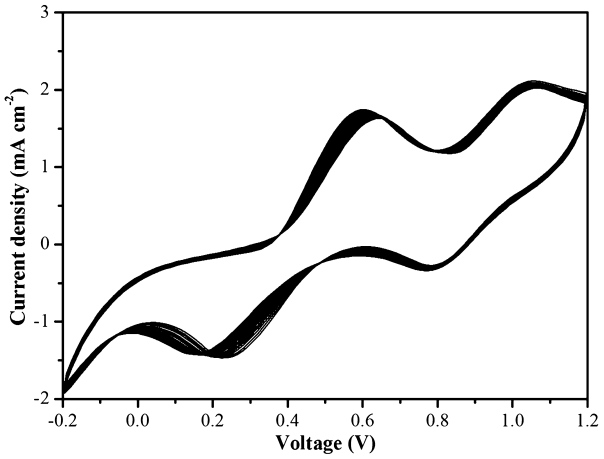

Figure 9. Consecutive 20 cyclic voltammograms for $Ni_{0.85}Se$@RGO CE at a scan rate of 25 mV s^{-1}.

but also high electrochemical stability. The high PCE and excellent chemical stability revealed that mesoporous $Ni_{0.85}Se$@RGO is a promising alternative to Pt electrode for DSSCs. The consecutive CV profiles of $Ni_{0.85}Se$, Pt, and RGO CEs are shown in Supporting Information, Figure S5.

4. CONCLUSION

In summary, mesoporous $Ni_{0.85}Se$@RGO nanocomposites were successfully synthesized through the hydrothermal method and yielded excellent performances in DSSC. Extensive electrochemical analyses demonstrated that mesoporous $Ni_{0.85}Se$@RGO nanocomposites owned high catalytic activity and fast electron-transport ability. These excellent electrocatalytic properties of $Ni_{0.85}Se$@RGO CE led to the reaction of the I_3^- reduction faster and more complete than that of Pt. Furthermore, photogenerated electron transfer at the CE/electrolyte interface got enhanced. These excellent abilities endowed $Ni_{0.85}Se$@RGO with higher current intensity than Pt and correspondingly higher PCE. The excellent photovoltaic property and chemical stability suggested that $Ni_{0.85}Se$@RGO could be an alternative to Pt electrode for DSSCs.

■ ASSOCIATED CONTENT

Supporting Information

SEM and TEM images of the mesoporous $Ni_{0.85}Se$@RGO nanospheres. SEM image of the mesoporous $Ni_{0.85}Se$ nanospheres. TEM image of as-prepared GO. Annotations of getting J_0 and J_{lim} from the Tafel curves. Consecutive 20 cyclic voltammograms for $Ni_{0.85}Se$, Pt, and RGO CEs at a scan rate of 25 mV s^{-1}. This material is available free of charge via the Internet at http://pubs.acs.org.

■ AUTHOR INFORMATION

Corresponding Authors

*E-mail: liul@nankai.edu.cn. (L.L.)
*E-mail: fzhu@nankai.edu.cn. (F.H.)

Notes

The authors declare no competing financial interest.

■ ACKNOWLEDGMENTS

This work was supported by the National Science Foundation of China (No. 21271108), Ministry of Science and Technology (Grant 2014CB932001) and China−U.S. Center for Environmental Remediation and Sustainable Development.

■ REFERENCES

(1) Xue, Y. H.; Liu, J.; Chen, H.; Wang, R. G.; Li, D. Q.; Qu, J.; Dai, L. M. Nitrogen-Doped Graphene Foams as Metal-Free Counter Electrodes in High-Performance Dye-Sensitized Solar Cells. *Angew. Chem., Int. Ed.* **2012**, *51*, 12124−12127.

(2) Wu, M. X.; Lin, X.; Wang, Y. D.; Wang, L.; Guo, W.; Qi, D. D.; Peng, X. J.; Hagfeldt, A.; Grätzel, M.; Ma, T. L. Economical Pt-Free Catalysts for Counter Electrodes of Dye-Sensitized Solar Cells. *J. Am. Chem. Soc.* **2012**, *134*, 3419−3428.

(3) Chang, S. H.; Lu, M. D.; Tung, Y. L.; Tuan, H. Y. Gram-Scale Synthesis of Catalytic Co_9S_8 Nanocrystal Ink as a Cathode Material for Spray-Deposited, Large Area Dye-Sensitized Solar Cells. *ACS Nano* **2013**, *7*, 9443−9451.

(4) Wang, H.; Hu, Y. H. Graphene as a Counter Electrode Material for Dye-Sensitized Solar Cells. *Energy Environ. Sci.* **2012**, *5*, 8182−8288.

(5) Yeh, M. H.; Lin, L. Y.; Sun, C. L.; Leu, Y. A.; Tsai, J. T.; Yeh, C. Y.; Vittal, R.; Ho, K. C. Multiwalled Carbon Nanotube@Reduced Graphene Oxide Nanoribbon as the Counter Electrode for Dye-Sensitized Solar Cells. *J. Phys. Chem. C* **2014**, *118*, 16626−16634.

(6) Wu, K. L.; Li, C. H.; Chi, Y.; Clifford, J. N.; Cabau, L.; Palomares, E.; Cheng, Y. M.; Pan, H. A.; Chou, P. T. Dye Molecular Structure Device Open-Circuit Voltage Correlation in Ru(II) Sensitizers with Heteroleptic Tridentate Chelates for Dye Sensitized Solar Cells. *J. Am. Chem. Soc.* **2012**, *134*, 7488−7496.

(7) Chen, H. J.; Xie, Y. A.; Cui, H. L.; Zhao, W.; Zhu, X. L.; Wang, Y. M.; Lu, X. J.; Huang, F. Q. In Situ Growth of a $MoSe_2$/Mo Counter Electrode for High Efficiency Dye-Sensitized Solar Cells. *Chem. Commun.* **2014**, *50*, 4475−4477.

(8) Wang, H.; Wei, W.; Hu, Y. H. NiO as an Efficient Counter Electrode Catalyst for Dye-Sensitized Solar Cells. *Top Catal.* **2014**, *57*, 607−611.

(9) Wei, W.; Wang, H.; Hu, Y. H. Unusual Particle-Size-Induced Promoter-to-Poison Transition of ZrN in Counter Electrodes for Dye-Sensitized Solar Cells. *J. Mater. Chem. A* **2013**, *1*, 14350−14357.

DOI: 10.1021/acsami.5b00464
ACS Appl. Mater. Interfaces 2015, 7, 8457−8464

(10) Wu, M. X.; Lin, X.; Hagfeldt, A.; Ma, T. L. Low-Cost Molybdenum Carbide and Tungsten Carbide Counter Electrodes for Dye-Sensitized Solar Cells. *Angew. Chem., Int. Ed.* **2011**, *50*, 3520−3524.
(11) Al-Mamun, M.; Zhang, H. M.; Liu, P. R.; Wang, Y.; Cao, J.; Zhao, H. J. Directly Hydrothermal Growth of Ultrathin MoS_2 Nanostructured Films as High-Performance Counter Electrodes for Dye-Sensitised Solar Cells. *RSC Adv.* **2014**, *4*, 21277−21283.
(12) Gong, F.; Wang, H.; Xu, X.; Zhou, G.; Wan, Z. S. In Situ Growth of $Co_{0.85}Se$ and $Ni_{0.85}Se$ on Conductive Substrates as High-Performance Counter Electrodes for Dye-Sensitized Solar Cells. *J. Am. Chem. Soc.* **2012**, *134*, 10953−10958.
(13) Wu, J. H.; Yue, G. T.; Xiao, Y. M.; Huang, M. L.; Lin, J. M.; Fan, L. Q.; Lan, Z.; Lin, J. Y. Glucose Aided Preparation of Tungsten Sulfide/Multi-Wall Carbon Nanotube Hybrid and Use as Counter Electrode in Dye-Sensitized Solar Cells. *ACS Appl. Mater. Interfaces* **2012**, *4*, 6530−6536.
(14) Ju, M. J.; Kim, J. C.; Choi, H. J.; Choi, I. T.; Kim, S. G.; Lim, K. M.; Ko, J. J.; Lee, J. J.; Jeon, I. Y.; Baek, J. B.; Kim, H. K. N−Doped Graphene Nanoplatelets as Superior Metal-Free Counter Electrodes for Organic Dye-Sensitized Solar Cells. *ACS Nano* **2013**, *7*, 5243−5250.
(15) Yang, Z. B.; Chen, T.; He, R. X.; Guan, G. Z.; Li, H. P.; Qiu, L. B.; Peng, H. S. Aligned Carbon Nanotube Sheets for the Electrodes of Organic Solar Cells. *Adv. Mater.* **2011**, *23*, 5436−5439.
(16) Sahoo, N. G.; Pan, Y. Z.; Li, L.; Chan, S. H. Graphene-Based Materials for Energy Conversion. *Adv. Mater.* **2012**, *24*, 4203−4210.
(17) Liu, H. W.; Liang, S. P.; Wu, T. J.; Chang, H. M.; Kao, P. K.; Hsu, C. C.; Chen, J. Z.; Chou, P. T.; Cheng, I. C. Rapid Atmospheric Pressure Plasma Jet Processed Reduced Graphene Oxide Counter Electrodes for Dye-Sensitized Solar Cells. *ACS Appl. Mater. Interfaces* **2014**, *6*, 15105−15112.
(18) Guai, G. H.; Leiw, M. Y.; Ng, C. M.; Li, C. M. Sulfur-Doped Nickel Oxide Thin Film as an Alternative to Pt for Dye-Sensitized Solar Cell Counter Electrodes. *Adv. Energy Mater.* **2012**, *2*, 334−338.
(19) Lin, X.; Wu, M. X.; Wang, Y. D.; Hagfeldt, A.; Ma, T. L. Novel Counter Electrode Catalysts of Niobium Oxides Supersede Pt for Dye-Sensitized Solar Cells. *Chem. Commun.* **2011**, *47*, 11489−11491.
(20) Xia, J. B.; Yuan, C. C.; Yanagida, S. Novel Counter Electrode V_2O_5/Al for Solid Dye-Sensitized Solar Cells. *ACS Appl. Mater. Interfaces* **2010**, *2*, 2136−2139.
(21) Li, G.; Chen, X. S.; Gao, G. D. Bi_2S_3 Microspheres Grown on Graphene Sheets as Low-cost Counter-electrode Materials for Dye Sensitized Solar Cells. *Nanoscale* **2014**, *6*, 3283−3288.
(22) Yang, J.; Bao, C. X.; Zhu, K.; Yu, T.; Li, F. M.; Liu, J. G.; Li, Z. S.; Zou, Z. G. High Catalytic Activity and Stability of Nickel Sulfide and Cobalt Sulfide Hierarchical Nanospheres on the Counter Electrodes for Dye-Sensitized Solar Cells. *Chem. Commun.* **2014**, *50*, 4824−4826.
(23) Kung, C. W.; Chen, H. W.; Lin, C. Y.; Huang, K. C.; Vittal, R.; Ho, K. C. CoS Acicular Nanorod Arrays for the Counter Electrode of an Efficient Dye-Sensitized Solar Cell. *ACS Nano* **2012**, *6*, 7016−7025.
(24) Wang, M. K.; Anghel, A. M.; Marsan, B.; Ha, N. L. C.; Pootrakulchote, N.; Zakeeruddin, S. M.; Grätzel, M. CoS Supersedes Pt as Efficient Electrocatalyst for Triiodide Reduction in Dye-Sensitized Solar Cells. *J. Am. Chem. Soc.* **2009**, *131*, 15976−15977.
(25) Li, G. R.; Wang, F.; Jiang, Q. W.; Gao, X. P.; Shen, P. W. Carbon Nanotubes with Titanium Nitride as a Low-Cost Counter-Electrode Material for Dye-Sensitized Solar Cells. *Angew. Chem., Int. Ed.* **2010**, *49*, 3653−3656.
(26) Jiang, Q. W.; Li, G. R.; Gao, X. P. Highly ordered TiN Nanotube Arrays as Counter Electrodes for Dye-Sensitized Solar Cells. *Chem. Commun.* **2009**, 6720−6722.
(27) Gong, F.; Xu, X.; Li, Z. Q.; Zhou, G.; Wang, Z. S. $NiSe_2$ as an Efficient Electrocatalyst for a Pt-Free Counter Electrode of Dye-Sensitized Solar Cells. *Chem. Commun.* **2013**, *49*, 1437−1439.
(28) Wang, W. J.; Pan, X.; Liu, W. Q.; Zhang, B.; Chen, H. W.; Fang, X. Q.; Yao, J. X.; Dai, S. Y. $FeSe_2$ Films with Controllable Morphologies as Efficient Counter Electrodes for Dye-sensitized Solar Cells. *Chem. Commun.* **2014**, *50*, 2618−2620.
(29) Wei, W.; Wang, H.; Hu, Y. H. A Review on PEDOT-Based Counter Electrodes for Dye-Sensitized Solar Cells. *Int. J. Energy Res.* **2014**, *38*, 1099−1111.
(30) Du, X.; Skachko, I.; Barker, A.; Andrei, E. Y. Approaching Ballistic Transport in Suspended Graphene. *Nat. Nanotechnol.* **2008**, *118*, 491−495.
(31) Wei, W.; Sun, K.; Hu, Y. H. Synthesis of 3D Cauliflower-Fungus-Like Graphene from CO_2 as a Highly Efficient Counter Electrode Material for Dye-Sensitized Solar Cells. *J. Mater. Chem. A* **2014**, *2*, 16842−16846.
(32) Unarunotai, S.; Murata, Y.; Chialvo, C. E.; Mason, N.; Petrov, I.; Nuzzo, R. G.; Moore, J. S.; Rogers, J. A. Conjugated Carbon Monolayer Membranes: Methods for Synthesis and Integration. *Adv. Mater.* **2010**, *22*, 1072−1077.
(33) Wang, H.; Hu, Y. H. Graphene as a Counter Electrode Material for Dye-Sensitized Solar Cells. *Energy Environ. Sci.* **2012**, *5*, 8182−8188.
(34) Wang, H.; Sun, K.; Tao, F.; Stacchiola, D. J.; Hu, Y. H. 3D Honeycomb-Like Structured Graphene and Its High Efficiency as a Counter-Electrode Catalyst for Dye-Sensitized Solar Cells. *Angew. Chem., Int. Ed.* **2013**, *52*, 9210−9214.
(35) Xu, F.; Chen, J.; Wu, X.; Zhang, Y.; Wang, Y. X.; Sun, J.; Bi, H. C.; Lei, W.; Ni, Y. R.; Sun, L. T. Graphene Scaffolds Enhanced Photogenerated Electron Transport in ZnO Photoanodes for High-Efficiency Dye-Sensitized Solar Cells. *J. Phys. Chem. C* **2013**, *117*, 8619−8627.
(36) Wang, H.; Leonard, S. L.; Hu, Y. H. Promoting Effect of Graphene on Dye-Sensitized Solar Cells. *Ind. Eng. Chem. Res.* **2012**, *51*, 10613−10620.
(37) Wang, R.; Wu, Q. D.; Lu, Y.; Liu, H. W.; Xia, Y. Z.; Liu, J. Q.; Yang, D. J.; Huo, Z. Y.; Yao, X. D. Preparation of Nitrogen-Doped TiO_2/Graphene Nanohybrids and Application as Counter Electrode for Dye-Sensitized Solar Cells. *ACS Appl. Mater. Interfaces* **2014**, *6*, 2118−2124.
(38) Ma, J.; Li, C.; Yu, F.; Chen, J. H. 3D Single-Walled Carbon Nanotube/Graphene Aerogels as Pt-Free Transparent Counter Electrodes for High Efficiency Dye-Sensitized Solar Cells. *ChemSusChem* **2014**, *7*, 3304−3311.
(39) Bajpai, R.; Roy, S.; Kulshrestha, N.; Rafiee, J.; Koratkar, N.; Misra, D. S. Graphene Supported Nickel Nanoparticle as a Viable Replacement for Platinum in Dye Sensitized Solar Cells. *Nanoscale* **2012**, *4*, 926−930.
(40) Bajpai, R.; Roy, S.; Kumar, P.; Bajpai, P.; Kulshrestha, N.; Rafiee, J.; Koratkar, N.; Misra, D. S. Graphene Supported Platinum Nanoparticle Counter-Electrode for Enhanced Performance of Dye-Sensitized Solar Cells. *ACS Appl. Mater. Interfaces* **2011**, *3*, 3884−3889.
(41) Wang, Z. W.; Xu, H. X.; Zhang, Z. Y.; Zhou, X. H.; Pang, S. P.; Cu, G. L. High-Performance Cobalt Selenide and Nickel Selenide Nanocomposite Counter Electrode for Both Iodide/Triiodide and Cobalt(II/III) Redox Couples in Dye-Sensitized Solar Cells. *Chin. J. Chem.* **2014**, *32*, 491−497.
(42) Lee, J. S.; Kim, S. I.; Yoon, J. C.; Jang, J. H. Chemical Vapor Deposition of Mesoporous Graphene Nanoballs for Supercapacitor. *ACS Nano* **2013**, *7*, 6047−6055.
(43) Yang, D. S.; Kim, C. W.; Song, M. Y.; Park, H. Y.; Kim, J. C.; Lee, J. J.; Ju, M. J.; Yu, J. S. N-Doped Hierarchical Hollow Mesoporous Carbon as Metal-Free Cathode for Dye-Sensitized Solar Cells. *J. Phys. Chem. C* **2014**, *118*, 16694−16702.
(44) Zhao, B.; Huang, H.; Jiang, P.; Zhao, H. F.; Huang, X. W.; Shen, P.; Wu, D. C.; Fu, R. W.; Tan, S. T. Flexible Counter Electrodes Based on Mesoporous Carbon Aerogel for High-Performance Dye-Sensitized Solar Cells. *J. Phys. Chem. C* **2011**, *115*, 22615−22621.
(45) Su, C. Y.; Xu, Y. P.; Zhang, W. J.; Zhao, J. W.; Tang, X. H.; Tsai, C. H.; Li, L. J. Electrical and Spectroscopic Characterizations of Ultra-Large Reduced Graphene Oxide Monolayers. *Chem. Mater.* **2009**, *21*, 5674−5680.

DOI: 10.1021/acsami.5b00464
ACS Appl. Mater. Interfaces 2015, 7, 8457−8464

(46) Zhuang, H. B.; Peng, Q.; Zhuang, J.; Wang, X.; Li, Y. D. Controlled Hydrothermal Synthesis and Structural Characterization of a Nickel Selenide Series. *Chem.—Eur. J.* **2006**, *12*, 211−217.
(47) Fan, Z.; Wang, K.; Wei, T.; Yan, J.; Song, L.; Shao, B. An Environmentally Friendly and Efficient Route for the Reduction of Graphene Oxide by Aluminum Powder. *Carbon* **2010**, *48*, 1686−1689.
(48) Yen, M. Y.; Teng, C. C.; Hsiao, M. C.; Liu, P. I.; Chuang, W. P.; Ma, C. C. M.; Hsieh, C. K.; Tsaib, M. C.; Tsai, C. H. Platinum Nanoparticles/Graphene Composite Catalyst as a Novel Composite Counter Electrode for High Performance Dye-Sensitized Solar Cells. *J. Mater. Chem.* **2011**, *21*, 12880−12888.
(49) Bai, Y.; Zong, X.; Yu, H.; Chen, Z. G.; Wang, L. Z. Scalable Low-Cost SnS_2 Nanosheets as Counter Electrode Building Blocks for Dye-Sensitized Solar Cells. *Chem.—Eur. J.* **2014**, *20*, 1−8.
(50) Guo, J. H.; Shi, Y. T.; Zhu, C.; Wang, L.; Wang, N.; Ma, T. L. Cost-Effective and Morphology-Controllable Niobium Diselenides for Highly Efficient Counter Electrodes of Dye-sensitized Solar Cells. *J. Mater. Chem. A* **2013**, *1*, 11874−11879.
(51) Li, Z. Q.; Gong, F.; Zhou, G.; Wang, Z. S. NiS_2/Reduced Graphene Oxide Nanocomposites for Efficient Dye-Sensitized Solar Cells. *J. Phys. Chem. C* **2013**, *117*, 6561−6566.
(52) Wang, H.; Wei, W.; Hu, Y. H. Efficient ZnO-Based Counter Electrodes for Dye-Sensitized Solar Cells. *J. Mater. Chem. A* **2013**, *1*, 6622−6628.
(53) Miao, X. H.; Pan, K.; Wang, G. F.; Liao, Y. P.; Wang, L.; Zhou, W.; Jiang, B. J.; Pan, Q. J.; Tia, G. H. Well-Dispersed CoS Nanoparticles on a Functionalized Graphene Nanosheet Surface: A Counter Electrode of Dye-Sensitized Solar Cells. *Chem.—Eur. J.* **2014**, *20*, 474−482.

DOI: 10.1021/acsami.5b00464
ACS Appl. Mater. Interfaces 2015, 7, 8457−8464